A Novel and Functionally Diverse Class of Acetylcholine-gated Ion Channels

Iris Hardege *[1], Julia Morud *[1], William R Schafer [1,2]

Affiliations

[1] MRC Laboratory of Molecular Biology, Francis Crick Avenue, Cambridge, CB2 0QH, United Kingdom

[2] Department of Biology, KU Leuven, Leuven, Belgium

* These authors contributed equally to this work

Corresponding Author: William R Schafer, wschafer@mrc-lmb.cam.ac.uk

Abstract

Fast cholinergic neurotransmission is mediated by pentameric acetylcholine-gated ion channels; in particular, cationic nicotinic acetylcholine receptors play well-established roles in virtually all nervous systems. Acetylcholine-gated anion channels have also been identified in some invertebrate phyla, yet their roles in the nervous system are less well-understood. Here we describe the functional properties of five previously-uncharacterized acetylcholine-gated anion channels from *C. elegans*, including four from a novel nematode specific subfamily known as the diverse group. In addition to their activation by acetylcholine, these diverse group channels are activated at physiological concentrations by other ligands; three, encoded by the *lgc-40*, *lgc-57* and *lgc-58* genes, are activated by choline, while *lgc-39* encoded channels are activated by octopamine and tyramine. Intriguingly, these and other acetylcholine-gated anion channels show extensive co-expression with cation-selective nicotinic receptors, implying that many cholinergic synapses may have both excitatory and inhibitory potential. Thus, the evolutionary expansion of cholinergic ligand-gated ion channels may enable complex synaptic signalling in an anatomically compact nervous system.

Keywords

Choline / *C.elegans* / Co-expression / Polymodal / Synaptic localisation

Introduction

Rapid signalling through neuronal networks is essential for producing coordinated behaviours in animals. At the fundamental level, fast neurotransmission is mediated through neurotransmitter release, resulting in activation of ion channels on the postsynaptic neuron. In the textbook view, based predominately on mammalian systems, there are two major excitatory

neurotransmitters, glutamate, and acetylcholine, and two inhibitory neurotransmitters, GABA and glycine. Glutamate acts through a family of tetrameric ligand-gated cation channels, while the remaining neurotransmitters activate pentameric receptors from the Cys-loop receptor superfamily of ligand-gated ion channels (LGICs). Although LGICs are highly conserved across phyla, ligand binding properties and ion selectivity diverge significantly, resulting in a large diversity of mechanisms by which small molecules acting via LGICs can influence the activity in neuronal circuits.

Despite their conserved general structure, Cys-loop LGICs vary significantly in their functional properties, particularly when channels from invertebrate phyla are considered. For example, insects and nematodes express inhibitory glutamate receptors from the Cys-loop superfamily, localised both in neurons and muscles, which are targets of the anthelminthic drug ivermectin (Cully *et al*, 1996, 1994). Many animals including insects, nematodes and mammals also express LGICs that can be gated by aminergic ligands, including histamine-gated chloride channels in *Drosophila* (Gisselmann *et al*, 2002), various nematode channels gated by dopamine, tyramine and serotonin (Morud *et al*, 2021; Pirri *et al*, 2009), as well as the excitatory mammalian 5-HT_3 receptors (Kondo *et al*, 2014; Lombaert *et al*, 2018). Even more divergent roles for LGICs have been identified in marine species, where LGICs gated by terpenes and chloroquine function as chemoreceptors in octopus (van Giesen *et al*, 2020).

Cys-loop channels can be subdivided into two large clades, the first containing the nicotinic receptors and their paralogues (including the 5HT-3 receptors), and the other containing channels more closely related to $GABA_A$ receptors (Jones & Sattelle, 2008). The *C. elegans* genome contains several subfamilies which appear to have diversified independently from vertebrate channels during evolution, leading to the existence of several nematode

50 specific LGIC subfamilies. The *C. elegans* genome contains a number of $GABA_A$-like
51 subfamilies, including genes encoding both anion and cation-selective channels (Ranganathan
52 *et al*, 2000; Jobson *et al*, 2015; Ringstad *et al*, 2009; Putrenko *et al*, 2005; Margie *et al*, 2013;
53 Yassin *et al*, 2001). One of these subgroups consists of genes for monoamine-gated channels
54 (both anion and cation selective), and a second subgroup consists of eight channels, four of
55 which are acetylcholine-gated anion channels and four that are still uncharacterized. A third
56 subfamily, known as the "diverse group" (Hobert, 2013), is largely uncharacterised; though
57 one member, LGC-40, has been reported to be a low affinity serotonin-gated channel also gated
58 by acetylcholine and choline (Ringstad *et al*, 2009), the properties of the remaining eight
59 channels in this subgroup, including their ligands, ion selectivity, and expression patterns, are
60 currently unknown.
61
62 Here we describe the deorphanisation and characterisation of five new *C. elegans*
63 LGICs activated by acetylcholine, including four members of the diverse subgroup. One of
64 these, LGC-39, forms a polymodal homomeric anion channel activated by acetylcholine as
65 well as by monoamines, while three others are activated by both choline and acetylcholine.
66 Using public single cell RNAseq expression data together with our new electrophysiological
67 data, we also predict the polarity of synapses in the worm connectome, as well as intracellular
68 localisation patterns for uncharacterized LGICs. These results highlight the unexpected
69 functional diversity of cholinergic signalling in the *C. elegans* nervous system.
70

71 # Results

72 **Deorphanisation of Uncharacterised LGICs Reveals Diversity of Cholinergic Channels**

73 The *C. elegans* genome encodes a diverse superfamily of pentameric ligand-gated ion
74 channels (LGICs), of which several subfamilies are poorly characterised. In particular the

75 diverse group, consisting of the GGR-1 (here renamed to LGC-57) and the LGC-45
76 subfamilies, together includes nine LGICs (Figure 1B), whose activating ligand and function
77 are largely unknown. To investigate the properties of these channels, we first expressed each
78 channel gene in *Xenopus* oocytes and tested for current activation during the perfusion of a
79 panel of neurotransmitters. Despite their homology to vertebrate $GABA_A$ and glycine receptors
80 (the source of the name GGR-1), we observed no activation of any members of the GGR-1
81 group (or LGC-45 group) by either GABA or glycine. Instead, we found three closely related
82 channels LGC-57 (aka GGR-1), LGC-58 (aka GGR-2) and LGC-40 that were specifically
83 gated by choline and acetylcholine (Figure 1A). All three channels showed a preference for
84 choline, with EC_{50} values 2.5 to 3-fold lower for choline than acetylcholine (Figure 1C). These
85 findings parallel a previous report that LGC-40 forms a choline and acetylcholine-gated
86 channel, although in contrast to that report we did not observe serotonin responses (Ringstad
87 *et al*, 2009). We did not observe currents in response to any of the tested compounds for the
88 remaining members of the LGC-57 group (LGC-41 and LGC-42) nor for any members of the
89 LGC-45 group (Figure S1A).
90
91 In addition to the LGC-57 and LGC-45 groups, many other *C. elegans* LGICs lack
92 identified ligands. While several members of the so-called ACC group of LGICs have been
93 shown to form acetylcholine-gated chloride channels, four members of this subfamily *(acc-4,*
94 *lgc-47, lgc-48,* and *lgc-49)* had not previously been characterised (Figure 1B*)*. Upon expression
95 in *Xenopus* oocytes, we found that one of these channels, LGC-49, formed an acetylcholine
96 gated channel with an EC_{50} of 19μM (Figure 1C). Unlike the members of the LGC-57 group,
97 LGC-49 showed no significant activation by choline. No ligand-induced currents were
98 observed for ACC-4, LGC-47 or LGC-48, either alone, or in combination with closely related
99 and previously characterised LGCs, such as ACC-1 (Figure S1A-B) (Putrenko *et al*, 2005).

100

101 We next investigated the ion selectivity of the newly-deorphanised channels by
102 carrying out ion substitution experiments in oocytes expressing LGC-57, LGC-58, LGC-40, or
103 LGC-49. For all channels we observed significant reversal potential shifts following
104 substitution of standard high NaCl buffer for low Cl (Na Gluconate), but not for substitution
105 with Na^+-free (NMDG) solution, indicating selectivity for anions over cations for all the tested
106 channels (Figure 2A-B). We also tested the previously deorphanised channel LGC-46 (Liu *et*
107 *al*, 2017), which to date lacked ion selectivity data; this likewise showed reversal shifts
108 characteristic of an anion selective channel (Figure 2A-B). Interestingly, all members of the
109 LGC-57 group possess a PAR motif (Proline-Alanine-Arginine), located in the M2-3
110 intracellular loop, which has been shown to impart anion selectivity to LGICs (Wotring *et al*,
111 2003). Although several uncharacterised members of the ACC group have sequences that
112 diverge from the PAR motif, both LGC-49 and LGC-46 contain the PAR motif sequence. Thus,
113 the PAR motif appears to correlate with anion selectivity in both the LGC-57 and ACC groups
114 of nematode acetylcholine-gated LGICs.

115

116 **Cholinergic Channels Display Diverse Antagonist Binding Properties**

117 In order to understand if there are further functional differences between the channels
118 deorphanised in this study, we exposed each channel to three cholinergic antagonists,
119 mecamylamine, strychnine and d-tubocurarine. Strychnine and d-tubocurarine have been
120 shown to compete with the full agonist for the ligand binding domain, although their binding
121 mechanisms vary between LGICs of different classes (Brams *et al*, 2011); in contrast,
122 mecamylamine has been shown to interact with the transmembrane regions of mammalian
123 nAChRs (Bondarenko *et al*, 2014). We saw that the antagonistic profile differed significantly
124 between the newly-deorphanised channels. For example, within the LGC-57 group the two

125 smallest antagonists, mecamylamine and strychnine, had a similar IC_{50} values for LGC-57,
126 LGC-58a and LGC-40 (Figure 2D). However, tubocurarine, the largest molecule of the
127 antagonists, displayed an 11-fold shift in IC_{50} for LGC-57 compared to LGC-58 and LGC-40
128 (Figure 2D). Thus, the binding capabilities of tubocurarine on LGC-57 differs substantially
129 from that of its closest family members LGC-58 and LGC-40. Likewise, in the ACC group,
130 LGC-46 and LGC-49 could both be blocked by mecamylamine and strychnine (Figure 2D);
131 LGC-49 could additionally be blocked by tubocurarine and picrotoxin. These dissimilarities
132 again highlight the discrete differences between channels from the same subfamily, which may
133 have similar ligand binding profiles for endogenous ligands. Interestingly, tubocurarine was
134 the most potent blocker for the ACC group channels LGC-46 and LGC-49, whereas this
135 antagonist was the least effective of those tested for the LGC-57 group channels.
136
137 We also tested the channels' responses to repeated stimulation by the endogenous
138 primary ligand. We found LGC-40 to be sensitive to repeated stimulation, displaying a
139 significant difference in ratio between the first and second pulse after both 10s of and 60 s of
140 washing intervals (Figure 2C). In contrast, all other channels were capable of fast activation
141 intervals as they did not display any decrease in peak amplitude after repeated stimulation
142 (Figure 2C). Thus, LGC-40 appears to desensitize more than the other channels following
143 activation by its ligand.
144
145 **LGC-39 is a Novel Polymodal Channel Activated by Cholinergic and Aminergic**
146 **Ligands**
147 One channel from the LGC-57 subfamily, LGC-39, showed distinct ligand binding
148 properties from the rest of the group. Unlike the other LGC-57 subfamily members, LGC-39
149 showed relatively little activation by choline. Moreover, while acetylcholine activated LGC-

150 39 channels strongly (with an EC_{50} of 1290μM), the most potent ligands for LGC-39 were the
151 monoamines octopamine and tyramine (with EC_{50} values of 921μM and 686μM respectively;
152 Figure 3A-B). In addition, LGC-39 also displayed small currents in response to dopamine
153 (Figure 3A). Like other members of the LGC-57 family, LGC-39 contains the PAR sequence,
154 and LGC-39-expressing oocytes showed reversal potential shifts in response to chloride but
155 not sodium substitution (Figure 3C). Thus, *lgc-39* appears to encode a homomeric anionic,
156 polymodal channel, capable of being activated by both aminergic and cholinergic
157 neurotransmitters (Figure 3A-C).
158
159 We tested the effects of antagonists on LGC-39 currents evoked by different activating
160 ligands. In the presence of acetylcholine, LGC-39 could be blocked by the antagonists
161 mecamylamine, strychnine and tubocurarine. In contrast, the octopamine response could not
162 be blocked by mecamylamine or strychnine. Surprisingly, strychnine, in the presence of
163 octopamine or without an activating ligand, acted as a partial agonist, inducing a small current
164 with an EC_{50} of 7.5μM (Figure 3D). These data suggest that the putative endogenous ligands
165 of LGC-39, acetylcholine and octopamine, may interact with and activate the receptor in
166 different manners. To further separate the functionality of the ligands, we also investigated if
167 repeated activation by the different ligands influenced the ability for reactivation of LGC-39
168 differently (Figure 3E). No difference was seen for any wash interval between the ligands,
169 which could suggest that all ligands occupy the binding site in a similar time frame or that the
170 recovery time for the receptor is independent of the activating ligand.
171
172 **Cholinergic Channels show Broad and Varied Expression in The *C. elegans* Nervous**
173 **System**

174 To gain insight into the roles of cholinergic LGICs in the nervous system, we generated
175 reporter lines to characterise their neural expression patterns. We used a similar set of
176 fluorescent reporter lines to characterise the expression pattern of the newly deorphanised
177 LGICs based transcriptional reporter transgenes in which the upstream promoter of the *lgc*
178 gene drives the expression of a fluorescent protein. We then identified transgene-expression
179 based upon location, morphology and known marker lines. Using such a transcriptional
180 reporter, we observed expression of *lgc-39* in a range of interneurons and motor neurons,
181 including the AVA premotor interneurons (Figure 4E). In addition to receiving extensive
182 cholinergic input, these neurons are the major synaptic target for the only octopaminergic
183 neurons, the RICs, suggesting that LGC-39 may be exposed to both octopamine and
184 acetylcholine *in vivo* (Figure 4F) and may be involved in both cholinergic and octopaminergic
185 synaptic transmission. For the rest of the LGC-57 group, we also observed primarily neuronal
186 expression, with little overlap observed in the neurons expressing reporters for *lgc-40, lgc-49*,
187 *lgc-57* and *lgc-58* (Figure 4A-D). This was particularly striking in motorneurons, with *lgc-40*
188 expressed in many pharyngeal neurons (M2, M3, MC, MI, I2), *lgc-49* in sensory neurons,
189 including posterior sensory neurons such as ALN and PLN, *lgc-57* in the A-class and B-class
190 motorneurons of the ventral cord, and *lgc-58* in the egg-laying motorneurons (VCs; *lgc-57* was
191 also observed in a subset of VCs) This suggests that these channels are likely to exist primarily
192 as homomers *in vivo* and function in distinct target neurons.
193
194 We also used reporters to analyse the expression pattern of several still-orphan LGICs,
195 including *lgc-42, lgc-47, lgc-48, lgc-43* and *lgc-45*, as well as the previously deorphanised
196 ACh-gated channel *lgc-46* (Takayanagi-Kiya *et al*, 2016) (Figure S2A). These reporters also
197 showed diverse and distinct patterns of expression, primarily in neurons. For example, *lgc-46*
198 was broadly expressed in several neurons, mostly in the head (Figure S2C). Most of the orphan

199 channels were also expressed specifically in neurons; for *lgc-47* this expression was unusually
200 broad, encompassing sensory, motor, and interneurons, while *lgc-48* was expressed only in a
201 single pair of ADL chemosensory neurons. Interestingly, two the orphan channels, *lgc-43,* and
202 *lgc-45,* which lack a PAR sequence and may thus encode cationic channels, did not appear to
203 be expressed in neuronal tissue, but instead in the hypodermis (Figure S2A). Together, these
204 data suggest that these channels play various roles in, and outside, the nervous system.
205
206 **Excitatory and Inhibitory ACh Receptors are Co-expressed in Many Neurons**
207 Our expression analysis indicated that many of the inhibitory ACh receptors newly
208 deorphanised in this study are expressed in neurons previously shown to also express excitatory
209 ACh receptors. These results imply that the role for acetylcholine as an inhibitory
210 neurotransmitter may be greater than previously assumed, and that acetylcholine contributes to
211 both inhibitory and excitatory events in many neurons. To determine the extent to which
212 excitatory and inhibitory receptors for the same neurotransmitter are expressed in individual
213 neural classes, we made use of single cell RNAseq dataset from *C. elegans* neurons (Taylor *et*
214 *al*, 2021). We first generated a complete list of ionotropic receptors for each of the three
215 classical neurotransmitters ACh, GABA and glutamate (Table S1). Since missing receptors
216 would have the potential to bias predictions, we predicted the ligand and ion selectivity of
217 orphan channels based upon homology with characterised channels and the presence or absence
218 of a PAR motif in the M2-3 intracellular loop (see Methods).
219
220 From this analysis, we found a remarkable frequency of neuron classes co-expressing
221 both inhibitory and excitatory receptors for the same neurotransmitter. This was particularly
222 notable for acetylcholine, with over 60% of neuron classes expressing both excitatory and
223 inhibitory ACh receptors. In contrast, GABA receptors were more biased toward inhibition,

224 with over 40% of neuron classes only expressing inhibitory GABA receptors (Figure 5A, S3).
225 To make generalised predictions of synaptic polarity, we summed expression of inhibitory and
226 excitatory receptors for each neurotransmitter in each neuron class and assigned synapse
227 polarity based on the most prevalent receptors in each neuron class, assuming that all receptors
228 in a cell are present equally at all synapses (Figure 5C, S4). This analysis suggested that the
229 majority of ACh and Glu synapses are excitatory and most GABA synapses inhibitory, though
230 this varied significantly for individual connections (Figure 5B).
231
232 **Determining Synaptic Localisation of LGICs**
233 We reasoned that the single cell RNAseq dataset (Taylor *et al*, 2021) might also be
234 useful for predicting the intracellular localization of cholinergic LGICs, as presynaptic
235 receptors would be predicted to be expressed in cholinergic neurons while postsynaptic
236 receptors should be expressed in neurons receiving cholinergic input. To assess the correlation
237 between the number of cholinergic synapses a neuron makes ('ACh out'), or receives ('ACh
238 in'), with the expression level of cholinergic LGICs, we produced two heatmaps representing
239 either ACh out (Figure 6A), or in (Figure 6B), correlated to transcript level (Figure S5). This
240 analysis identified some receptors, such as *lgc-49*, that were primarily expressed in neurons
241 that receive a high number of cholinergic synapses (VD, DD; Figure 6C), consistent with a
242 postsynaptic receptor. Other channels were primarily expressed in neurons that make many
243 cholinergic synapses, such as *acc-1* in SMB and SAB (Figure 6D), consistent with presynaptic
244 localization. Others, such as *lgc-40* showed little correlation to cholinergic in- or out-degree
245 (Figure 6E), suggesting extrasynaptic localization and function or as for *lgc-46* a similar
246 correlation between in or out degree (Figure 6F).
247

248 To empirically assess the synaptic localization of cholinergic LGICs, we generated
249 endogenous GFP-tagged CRISPR lines for members of the LGC-57 subgroup, including *lgc-*
250 *39*, *lgc-40, lgc-57,* and *lgc-58* and (Figure 7A-D). In all cases GFP was inserted in the
251 intracellular M3/4 loop and the function of the resulting chimeric protein was verified in
252 *Xenopus* oocytes (Figure S6A). We observed a clear difference in the localisation patterns for
253 these channels. LGC-39::GFP was localised in distinct punctate structures both in the nerve
254 ring and along the ventral cord, suggestive of synaptic localisation (Figure 7A) and consistent
255 with the positive correlation between *lgc-39* expression and cholinergic in-degree. In contrast,
256 LGC-40::GFP appeared to have a diffuse nerve ring and touch receptor neuron GFP signal
257 (Figure 7B), with cell bodies often being visible, while LGC-57::GFP was found to be very
258 lowly expressed and little protein expression could be localised (Figure 7C). LGC-58::GFP
259 showed a clear nerve ring and VC4/5 localisation, including some punctate structures; since
260 LCG-58 showed a small but significant positive correlation with cholinergic out-decree, this
261 may indicate presynaptic localization (Figure 7D). Together, these results suggest that LGC-
262 39 receptors may be postsynaptic, while LGC-40, LGC-57 and LGC-58 may be primarily
263 extrasynaptic and/or presynyaptic.
264

265 # Discussion

266 **A Novel Family of Cholinergic LGICs**

267 This study highlights the diversity among cholinergic LGICs in *C. elegans*. Nematodes
268 have previously been shown to contain excitatory LGICs related to nicotinic receptors, as well
269 as inhibitory acetylcholine-gated chloride channels of the ACC family. Here we describe a new
270 subfamily of cholinergic LGICs, four of which form homomeric acetylcholine-gated anion
271 channels. In contrast to the previously described ACC subfamily of acetylcholine-gated anion
272 channels, three of these newly deorphanised channels (LGC-57, LGC-58 and LGC-40) are

273 gated preferentially by choline, the metabolite of acetylcholine which is abundant at
274 cholinergic synapses.
275
276 These results add to the already-extensive catalogue of acetylcholine-gated channels in
277 *C. elegans* (Yassin *et al*, 2001; Putrenko *et al*, 2005; Takayanagi-Kiya *et al*, 2016), highlighting
278 the expansion and importance of cholinergic transmission in nematodes. These newly
279 deorphanised channels display subtle variations in their ability to bind ligands and antagonists,
280 which translates into physiologically relevant differences that may increase the fine tuning in
281 the control of neuronal transmission and contribute to complex neuronal signalling within a
282 relatively minimal neuronal network. Interestingly, the electrophysiologically similar channels
283 LGC-57, LGC-58, and LGC-40 show largely distinct patterns of expression within the nervous
284 system of *C. elegans*, suggesting they may form homomeric channels with distinct functions
285 *in vivo*. When tagged with a fluorescent protein, these three channels also showed a diffuse
286 pattern of localisation within the neuron, suggesting that in contrast to ACC group channels
287 such as LGC-46 (Takayanagi-Kiya *et al*, 2016), they may not be synaptically localised. This
288 suggests a possible distinct extrasynaptic role for choline acting via these channels in the
289 modulation of the nervous system.
290
291 Our results raise the intriguing possibility that choline itself may function as a
292 neuromodulator. The idea that choline could activate cholinergic receptors independently from
293 acetylcholine has been discussed for other cholinergic receptors based on choline's ability to
294 dose-dependently either block or activate nicotinic channels (Purohit & Grosman, 2006).
295 However, the importance of choline activation to the *in vivo* functions of these channels has
296 remained unclear. Here we have identified three cholinergic receptors, LGC-40, LGC-57 and
297 LGC-58, in which choline acts as a full agonist, showing preference in binding and activation

298 degree for choline over acetylcholine. Previous reports show that in mammalian
299 neuromuscular AChRs, aromatic residues in the extracellular domain play a vital part in
300 stabilising the binding of acetylcholine over the binding to choline (Bruhova & Auerbach,
301 2017); interestingly, at least some of these aromatic residues are lacking in the choline-gated
302 receptors identified here. This suggests that LGC-40, LGC-57 and LGC-58 may in fact be
303 optimized for activation by choline rather than acetylcholine. Thus, it is not unreasonable to
304 hypothesise that choline could be an authentic endogenous ligand for these LGC-57-group
305 channels in *vivo*.

306

307 **A Polymodal LGIC Activated by Both Aminergic and Cholinergic Ligands**

308 In this study we also identified a novel polymodal channel, LGC-39, which is gated not
309 only by acetylcholine but also by the aminergic ligands tyramine and octopamine. The
310 expression pattern of *lgc-39* suggests that the channel might be exposed to all these ligands *in*
311 *vivo*. For example, *lgc-39* is highly expressed in the AVA premotor neurons, which receive a
312 many synapses from acetylcholine producing neurons (White, 1986) as well as from the RICs,
313 the only octopamine producing cells in the nervous system (Alkema & Horvitz, 1999). The
314 AVA neurons also receive some input from tyraminergic and dopaminergic neurons,
315 transmitters which we also found can activate LGC-39. Interestingly, in contrast to the choline-
316 gated channels LGC-40, LGC-57, and LGC-58, we observe clear punctate localisation of LGC-
317 39 in both the nerve ring and ventral cord, with no fluorescence visible in the cell bodies. This
318 may suggest a role for LGC-39 channels as postsynaptic receptors for both cholinergic and
319 aminergic neurotransmission.

320

321 The concept of a truly polymodal receptor has not before been investigated in great
322 detail, though previous observations have described roles for receptors that can use dual
323 ligands. For example dopamine exhibits a pseudo competitive ability to antagonise $GABA_A$

324 currents (Hoerbelt *et al*, 2015), while D-serine can function as an allosteric modulator of
325 NMDA receptor activity (Wolosker & Balu, 2020). Based on their capability to achieve dose-
326 dependent activation, both amines and acetylcholine appear to be true ligands of LGC-39, most
327 likely binding the ligand-binding domain. Understanding the mechanisms by which these
328 multiple neurotransmitters can activate LGC-39 and potentially affect different behavioural
329 outputs will be of interest in future studies.
330

331 **Functional Insights into The *C. elegans* Connectome**

332 With increasing molecular and physiological characterisation of neurotransmitter
333 receptors in *C. elegans*, it is becoming feasible to predict the functionality of synapses more
334 accurately in the *C. elegans* connectome. In this study we used the expression pattern of newly
335 and previously deorphanised LGICs for the three classical neurotransmitters, ACh, glutamate
336 and GABA, to predict the polarity of synapses in the *C. elegans* connectome. By assigning
337 synapse polarity based on the relative expression levels of anionic and cationic receptors, we
338 have provisionally predicted the sign of chemical synapses involving classical
339 neurotransmitters. Although similar attempts have been made in the past to assign polarity to
340 *C. elegans* synapses (Fenyves *et al*, 2020), these predictions were based upon incomplete or
341 incorrect ligand assignment for many LGICs. These revised predictions correlate well with
342 experimental data for many well-characterised circuits, such as the excitatory connections
343 between the ASH nociceptors and the AVA interneurons, as well as between the AVAs and
344 the VA and DA motorneurons (Mellem *et al*, 2002; Piggott *et al*, 2011). Predicted inhibitory
345 connections between AVB and AVA interneurons also correspond with empirical data on the
346 locomotor circuit (Kawano *et al*, 2011; Qi *et al*, 2012). Other predictions were counterintuitive;
347 for example, inhibitory connections were predicted between the AVDs and AVAs, two

348 interneuron pairs thought to be co-ordinately active during reverse locomotion (Faumont *et al*,
349 2012). Our predictions thus generate interesting functional hypotheses for future investigation.
350
351 A surprising outcome of the expression analysis was the high frequency with which
352 neurons expressed cationic and anionic receptors for the same neurotransmitter. This was
353 especially prevalent for acetylcholine; our analysis indicated that 60% of neuron classes
354 express both inhibitory and excitatory receptors for acetylcholine, 30% for glutamate and 10%
355 for GABA. One explanation for this apparent paradox is that excitatory and inhibitory receptors
356 might be differentially localised in neurons, with some found extrasynaptically and others
357 enriched in at synapses. Various *C. elegans* LGICs are known to act in regions other than the
358 post-synapse; for example *lgc-35* has been shown to mediate GABA spill-over transmission
359 (Jobson *et al*, 2015), while *lgc-46* appears be localised to the pre-synapse as an autoreceptor
360 (Takayanagi-Kiya *et al*, 2016). The choline-sensitive channels from the LGC-57 group
361 likewise appear to be extrasynaptic in their localization (Figure 7). In addition, postsynaptic
362 sites might themselves contain a mixture of excitatory and inhibitory receptors, which could
363 differ in their ligand affinity, desensitization kinetics and regulation. Indeed, LGIC localisation
364 is not static; for example, glutamatergic AMPA receptors have been shown in many species to
365 increase their synaptic localisation during learning (Malinow & Malenka, 2002), and recent
366 evidence indicates that *C. elegans* LGICs also display regulated membrane trafficking upon
367 learning (Morud *et al*, 2021). Thus, *C. elegans* may contain large numbers of complex
368 cholinergic synapses with the potential to be excitatory or inhibitory depending on context or
369 experience.
370

371 # Materials and Methods

372 ## *C. elegans* culture

373 Unless otherwise specified, *C. elegans* worms were cultured on NGM agar plates with OP50
374 (Stiernagle, 2006). A full list of strains used in this study can be found in table S1.
375

376 ## *Xenopus laevis* oocytes

377 Defolliculated *Xenopus laevis* oocytes were obtained from EcoCyte Bioscience (Dortmund,
378 Germany) and in ND96 (in mM: 96 NaCl, 1 $MgCl_2$, 5 HEPES, 1.8 $CaCl_2$, 2 KCl) solution at
379 16° C for 3-7 days.

380 ## Molecular biology

381 Unless otherwise specified, cDNA sequences of *C. elegans* genes were cloned from wildtype
382 N2 worm cDNA (generated by reverse transcription PCR from total worm RNA using Q5
383 polymerase (New England Biosciences)). Where multiple isoforms are present isoform a was
384 used. LGC-39 cDNA was generated by gene synthesis (ThermoFischer). For expression in
385 *Xenopus* oocytes, ion channel cDNA sequences were cloned into the KSM vector downstream
386 of a T3 promoter and between *Xenopus* β-globin 5' and 3'UTR regions using the HiFi
387 assembly protocol (New England Biosciences). *C. elegans* expression constructs were also
388 generated using the HiFi assembly protocol (New England Biosciences) into the
389 pDESTR4R3II backbone. *C. elegans* gDNA sequences were cloned from wildtype N2 gDNA
390 and expression verified by the addition of GFP or mKate2 introduced on the same plasmid after
391 an intercistronic splice site (SL2 site). Unless otherwise specified promoter sequences consist
392 of approximately 2kb of gDNA upstream of the start codon.
393

394 ## CRISPR/CAS9-mediated gene manipulation

395 Endogenous tagging of the M3/4 cytosolic loop of *C. elegans* LGIC proteins with GFP was
396 carried out either using the SapTrap protocol (Schwartz & Jorgensen, 2016; Dickinson *et al*,

397 2018) for *lgc-39(lj121)*, or by SunyBiotech (Fuzhou, China) for *lgc-57(syb3536)*, *lgc-*
398 *58(syb3562)*, and *lgc-40(syb3594)*.
399

400 **RNA synthesis and microinjection**

401 cRNA was synthesised *in vitro* using the T3 mMessage mMachine transcription kit according
402 to manufacturer's protocol to include a 5' cap (ThermoFischer Scientific). Prior to injection
403 RNA was purified using the GeneJET RNA purification kit (Thermo Fischer Scientific). Size
404 sorted and defolliculated *Xenopus* oocytes (Ecocyte) were placed individually into 96-well
405 plates and injected with 50 nL of 500 ng/μL RNA using the Roboinject system (Multi Channel
406 Systems GmbH). When two constructs were co-injected the total RNA concentration remained
407 500 ng/μL, with a 1:1 ratio of the components. Injected oocytes were incubated at 16°C in
408 ND96 until the day of recording, typically between 3-6 days post injection.
409

410 **Two-Electrode Voltage Clamp (TEVC) recording and data analysis**

411 Two-electrode voltage clamp recordings were carried out using either the Robocyte2 system
412 or a manual set up with an OC-725D amplifier (Multi Channel Systems GmbH). Glass
413 electrodes with a resistance ranging from 0.7-2 MΩ were pulled on a P1000 Micropipette Puller
414 (Sutter). Electrodes contained AgCl wires and backfilled with a 1.5M KCl and 1 M acetic
415 mixture. Unless otherwise stated, oocytes were clamped at -60mV. Continuous recordings at
416 500Hz were taken during application of a panel of agonists or antagonists. Data was recorded
417 using the RoboCyte2 control software, or with WinWCP for manual recordings, and filtered at
418 10 Hz.
419

420 Dose response protocols used 10s agonist application pulses with 60s of wash in ND96 between
421 each dose. Data was gathered over at least two occasions, using different batches of oocytes.

422 Peak current for each dose was normalised to the oocyte maximum current using a custom-
423 built python script (Morud *et al*, 2021). Normalised data was imported into Graphpad (Prism)
424 and fitted to either a three or four parameter nonlinear Hill equation to obtain the highest degree
425 of fit and calculate the EC_{50}. Antagonist dose responses and ion selectivity recordings were
426 carried out using the EC_{50} concentration of the primary agonist. Antagonist dose response
427 protocols used 10s agonist + antagonist windows, with 60s of ND96 washes between doses.
428 The agonist concentrations remained constant. Antagonist IC_{50} values were calculated using a
429 second custom built python script (Morud *et al*, 2021). Normalised data was imported into
430 Graphpad (Prism) and fitted to either a three or four parameter nonlinear Hill equation to obtain
431 the highest degree of fit and calculate the IC_{50}.
432
433 Ion selectivity was detected using a voltage ramp protocol from -80mV to +60mV (20mV/s)
434 in the presence of the primary agonist in three different solutions: ND96, NMDG (Na^+ free)
435 and Na Gluconate (low Cl^-) solutions. Data was normalised to max current and ΔE_{Rev} was
436 calculated using a custom-built python script (Morud *et al*, 2021). The resulting individual
437 values or mean, SD and n for each construct was imported in GraphPad for further plotting and
438 statistical analysis. Statistically significant differences in ΔE_{Rev} were calculated in GraphPad
439 using a two-way ANOVA with Tukey's correction for multiple comparisons. A representative
440 normalised trace for each construct was also generated in Graphpad.
441

442 **Confocal and Cell ID**

443 Worms were prepared and immobilised with 75 mM NaAzide in M9 and mounted onto 2%
444 agarose in M9 pads. Image stacks were acquired with a 63x water immersion lens on a Leica
445 SP8 or STED or using a 40x oil immersion objective on a Zeiss LSM780. Collapsed z-stack
446 images were generated in Fiji/Image J. Neurons expressing fluorescent reporters were

447 identified by cell shape, position and crossing with the multicolour reference worm NeuroPAL
448 (Yemini *et al*, 2020).
449

450 **Synaptic polarity prediction**

451 Inhibitory and excitatory chemical synapse prediction for ACh, Glu and GABA synapses were
452 made based upon expression levels of appropriate LGICs in postsynaptic cells. Chemical and
453 electrical connectome data was obtained from Wormweb (http://wormweb.org/details.html),
454 LGIC expression data was taken from the Cengen project using threshold level 4 (Taylor *et al*,
455 2021), ligand and selectivity for each channel was based upon this work, previous work and
456 predictions, a full list can be found in Table 1. Binary expression of LGICs for each
457 neurotransmitter in each neuron class were made based upon expression and characterised in
458 four groups: only excitatory, only inhibitory, both excitatory and inhibitory or none. These
459 binary values were used to make the binary expression heatmap. Overall polarity of a synapse
460 was calculated by summing the expression of all inhibitory and all excitatory LGICs for a given
461 neurotransmitter in each cell class. The sum inhibitory was then taken from the sum of
462 excitatory expression, resulting in an overall positive or negative signed expression in each
463 neuron class for each neurotransmitter. The ratio of these sums was also calculated to indicate
464 the strength of polarity. It was assumed that each LGIC in each neuron class is present equally
465 in all synapses, therefore each incoming connection could be assigned a polarity based upon
466 its receptor expression for that neurotransmitter. The resulting network with polarity was
467 imported into cystoscope (Shannon *et al*, 2003) for plotting and further analysis. Analysis
468 scripts can be found on GitHub at hiris25/Worm-Connectome-Polarity.
469

470 **Expression and cholinergic synapse analysis**

471 The total number of cholinergic input or output synapses was calculated for each neuronal class
472 by summing the number of presynapses for each cell that received a synapse from an ACh-
473 producing neuron (receiving synapses), or the total number of post-synapses an ACh-producing
474 neuron class makes (sending synapses). Acetylcholine producing cells were described by
475 (Pereira *et al*, 2015), the assumption was that all synapses made by an ACh-producing cell also
476 release ACh, even when this cell co-transmits another neurotransmitter. Synapse number for
477 each neuron was taken from (White, 1986). Expression data was obtained from (Taylor *et al*,
478 2020) using a stringent threshold of 4. Neuronal classes were sorted by ACh in or out degree
479 and the expression of each gene was mapped using a heatmap with an upper threshold of 500.
480 Correlation between expression level and ACh in, or out, degree was mapped using relplot in
481 python's seaborn package, confidence intervals were placed at 68%, corresponding to the
482 standard error of the estimate.
483

484 **Data analysis**

485 Unless otherwise specified data was imported into GraphPad for further analysis and plotting.
486 Unless otherwise specified, one-way ANOVA was used to calculate significant differences,
487 using the Bonferroni (food leaving & dispersal) or Tukey's (food leaving time course,
488 chemotaxis) correction for multiple comparisons. *= P<0.05, **= P<0.005, ***=P<0.001,
489 ****P<0.0001.
490

491 **Data Availability**

492 Python scripts can be found at on GitHub at hiris25/TEVC-analysis-scripts and hiris25/Worm-
493 Connectome-Polarity. Aggregated data used for analysing TEVC data are available upon
494 request from the Lead Contact. Further information and requests for *C. elegans* strains and

495 plasmids is to be sent to and will be fulfilled by the Lead Contact William R Schafer,
496 wschafer@mrc-lmb.cam.ac.uk

497

498 **Acknowledgements**

499 The authors gratefully acknowledge Denise Walker and Lidia Ripoll Sanchez for help with
500 cloning design, help with generating and maintaining strains, and other past and present
501 members of the Schafer lab for helpful discussions. We would like to acknowledge the Centre
502 for Cellular Imaging at the University of Gothenburg, Sweden, and the National Microscopy
503 Infrastructure, NMI (NMI01125), for providing imaging facilities. This work was supported
504 by grants from the Medical Research Council (MC-A023-5PB91), the Wellcome Trust
505 (WT103784MA), National Institute of Health (W.R.S.), the Swedish Research council
506 (VR2017-00236), Knut and Alice Wallenberg foundation (KAW2019,0293), Bollan stipend,
507 Lundgrenska stiftelserna and Magnus Bergvalls Stiftelse (J.M.).

508

509 **Author Contributions**

510 I.H., J.M. and W.R.S. designed the experiments. I.H., J.M., performed experiments and
511 analysed data. I.H., J.M. and W.R.S. wrote the manuscript and all authors read and critically
512 revised the manuscript to its final form.

513

514 **Conflicts of Interest**

515 The authors declare no competing interests.

516

517 **References**

518 Alkema M & Horvitz B (1999) Determining the roles of octopamine and CREB in worm

519 behavior. *Int C elegans Meet* [PREPRINT]

520 Bondarenko V, Targowska-Duda KM, Jozwiak K, Tang P & Arias HR (2014) Molecular
521 interactions between mecamylamine enantiomers and the transmembrane domain of the
522 human α4β2 nicotinic receptor. *Biochemistry* 53

523 Brams M, Pandya A, Kuzmin D, van Elk R, Krijnen L, Yakel JL, Tsetlin V, Smit AB &
524 Ulens C (2011) A structural and mutagenic blueprint for molecular recognition of
525 strychnine and d-tubocurarine by different Cys-loop receptors. *PLoS Biol* 9

526 Bruhova I & Auerbach A (2017) Molecular recognition at cholinergic synapses:
527 acetylcholine versus choline. *J Physiol* 595

528 Cully DF, Paress PS, Liu KK, Schaeffer JM & Arena JP (1996) Identification of a Drosophila
529 melanogaster glutamate-gated chloride channel sensitive to the antiparasitic agent
530 avermectin. *J Biol Chem*

531 Cully DF, Vassilatis DK, Liu KK, Paress PS, Van Der Ploeg LHT, Schaeffer JM & Arena JP
532 (1994) Cloning of an avermectin-sensitive glutamate-gated chloride channel from
533 Caenorhabditis elegans. *Nature*

534 Dickinson D, Slabodnick M, Chen A & Goldstein B (2018) SapTrap assembly of repair
535 templates for Cas9-triggered homologous recombination with a self-excising cassette.
536 *microPublication Biol* 2018

537 Faumont S, Lindsay TH & Lockery SR (2012) Neuronal microcircuits for decision making in
538 C. elegans. *Curr Opin Neurobiol* 22 doi:10.1016/j.conb.2012.05.005 [PREPRINT]

539 Fenyves BG, Szilágyi GS, Vassy Z, Sőti C & Csermely P (2020) Synaptic polarity and sign-
540 balance prediction using gene expression data in the Caenorhabditis elegans chemical
541 synapse neuronal connectome network. *PLoS Comput Biol* 16

542 van Giesen L, Kilian PB, Allard CAH & Bellono NW (2020) Molecular Basis of
543 Chemotactile Sensation in Octopus. *Cell*

544 Gisselmann G, Pusch H, Hovemann BT & Hatt H (2002) Two cDNAS coding for histamine-
545 gated ion channels in D. melanogaster. *Nat Neurosci*
546 Hobert O (2013) The neuronal genome of Caenorhabditis elegans. *WormBook*
547 doi:10.1895/wormbook.1.161.1 [PREPRINT]
548 Hoerbelt P, Lindsley TA & Fleck MW (2015) Dopamine directly modulates GABAA
549 receptors. *J Neurosci* 35
550 Jobson MA, Valdez CM, Gardner J, Garcia LR, Jorgensen EM & Beg AA (2015) Spillover
551 transmission is mediated by the excitatory GABA receptor LGC-35 in C. elegans. *J*
552 *Neurosci*
553 Jones AK & Sattelle DB (2008) The cys-loop ligand-gated ion channel gene superfamily of
554 the nematode, Caenorhabditis elegans. *Invertebr Neurosci* 8: 41–47
555 Kawano T, Po MD, Gao S, Leung G, Ryu WS & Zhen M (2011) An imbalancing act: Gap
556 junctions reduce the backward motor circuit activity to bias C. elegans for forward
557 locomotion. *Neuron* 72
558 Kondo M, Nakamura Y, Ishida Y, Yamada T & Shimada S (2014) The 5-HT3A receptor is
559 essential for fear extinction. *Learn Mem* 21
560 Liu P, Chen B, Mailler R & Wang ZW (2017) Antidromic-rectifying gap junctions amplify
561 chemical transmission at functionally mixed electrical-chemical synapses. *Nat Commun*
562 Lombaert N, Hennes M, Gilissen S, Schevenels G, Aerts L, Vanlaer R, Geenen L, Van
563 Eeckhaut A, Smolders I, Nys J, *et al* (2018) 5-HTR 2A and 5-HTR 3A but not 5-HTR
564 1A antagonism impairs the cross-modal reactivation of deprived visual cortex in
565 adulthood. *Mol Brain* 11
566 Malinow R & Malenka RC (2002) AMPA receptor trafficking and synaptic plasticity. *Annu*
567 *Rev Neurosci* 25: 103–126 doi:10.1146/annurev.neuro.25.112701.142758 [PREPRINT]
568 Margie O, Palmer C & Chin-Sang I (2013) C. elegans chemotaxis assay. *J Vis Exp*

569 Mellem JE, Brockie PJ, Zheng Y, Madsen DM & Maricq A V. (2002) Decoding of
570 polymodal sensory stimuli by postsynaptic glutamate receptors in C. elegans. *Neuron* 36
571 Morud J, Hardege I, Liu H, Wu T, Choi M-K, Basu S, Zhang Y & Schafer WR (2021)
572 Deorphanization of novel biogenic amine-gated ion channels identifies a new serotonin
573 receptor for learning. *Curr Biol*
574 Pereira L, Kratsios P, Serrano-Saiz E, Sheftel H, Mayo AE, Hall DH, White JG, LeBoeuf B,
575 Garcia LR, Alon U, *et al* (2015) A cellular and regulatory map of the cholinergic
576 nervous system of C. Elegans. *Elife* 4
577 Piggott BJ, Liu J, Feng Z, Wescott SA & Xu XZS (2011) The neural circuits and synaptic
578 mechanisms underlying motor initiation in C. elegans. *Cell* 147
579 Pirri JK, McPherson AD, Donnelly JL, Francis MM & Alkema MJ (2009) A Tyramine-Gated
580 Chloride Channel Coordinates Distinct Motor Programs of a Caenorhabditis elegans
581 Escape Response. *Neuron* 62
582 Purohit Y & Grosman C (2006) Block of muscle nicotinic receptors by choline suggests that
583 the activation and desensitization gates act as distinct molecular entities. *J Gen Physiol*
584 127
585 Putrenko I, Zakikhani M & Dent JA (2005) A family of acetylcholine-gated chloride channel
586 subunits in Caenorhabditis elegans. *J Biol Chem* 280
587 Qi YB, Garren EJ, Shu X, Tsien RY & Jin Y (2012) Photo-inducible cell ablation in
588 Caenorhabditis elegans using the genetically encoded singlet oxygen generating protein
589 miniSOG. *Proc Natl Acad Sci U S A* 109
590 Ranganathan R, Cannon SC & Horvitz HR (2000) MOD-1 is a serotonin-gated chloride
591 channel that modulates locomotory behaviour in C. elegans. *Nature* 408
592 Ringstad N, Abe N & Horvitz HR (2009) Ligand-gated chloride channels are receptors for
593 biogenic amines in C. Elegans. *Science (80-)* 325

594 Schwartz ML & Jorgensen EM (2016) SapTrap, a toolkit for high-throughput CRISPR/Cas9
595 gene modification in Caenorhabditis elegans. *Genetics* 202
596 Shannon P, Markiel A, Ozier O, Baliga NS, Wang JT, Ramage D, Amin N, Schwikowski B
597 & Ideker T (2003) Cytoscape: A software Environment for integrated models of
598 biomolecular interaction networks. *Genome Res* 13
599 Stiernagle T (2006) Maintenance of C. elegans. *WormBook* doi:10.1895/wormbook.1.101.1
600 [PREPRINT]
601 Takayanagi-Kiya S, Zhou K & Jin Y (2016) Release-dependent feedback inhibition by a
602 presynaptically localized ligand-gated anion channel. *Elife*
603 Taylor SR, Santpere G, Weinreb A, Barrett A, Reilly MB, Xu C, Varol E, Oikonomou P,
604 Glenwinkel L, McWhirter R, *et al* (2020) Molecular topography of an entire nervous
605 system. *bioRxiv* doi:10.1101/2020.12.15.422897 [PREPRINT]
606 Taylor SR, Santpere G, Weinreb A, Barrett A, Reilly MB, Xu C, Varol E, Oikonomou P,
607 Glenwinkel L, McWhirter R, *et al* (2021) Molecular topography of an entire nervous
608 system. *Cell* 184
609 White JG. (1986) The structure of the nervous system of the nematode Caenorhabditis
610 elegans. *Philos Trans R Soc London B, Biol Sci* 314: 1–340
611 Wolosker H & Balu DT (2020) d-Serine as the gatekeeper of NMDA receptor activity:
612 implications for the pharmacologic management of anxiety disorders. *Transl Psychiatry*
613 10 doi:10.1038/s41398-020-00870-x [PREPRINT]
614 Wotring VE, Miller TS & Weiss DS (2003) Mutations at the GABA receptor selectivity
615 filter: A possible role for effective charges. *J Physiol* 548
616 Yassin L, Gillo B, Kahan T, Halevi S, Eshel M & Treinin M (2001) Characterization of the
617 DEG-3/DES-2 receptor: A nicotinic acetylcholine receptor that mutates to cause
618 neuronal degeneration. *Mol Cell Neurosci* 17

619 Yemini E, Lin A, Nejatbakhsh A, Varol E, Sun R, Mena GE, Samuel ADT, Paninski L,
620 Venkatachalam V & Hobert O (2020) NeuroPAL: A Multicolor Atlas for Whole-Brain
621 Neuronal Identification in C. elegans. *Cell*
622

623 ## Figure Legends

624

625 **Figure 1. Deorphanisation of Cholinergic Ligand Gated Ion Channels.** (**A**) Continuous
626 current traces of *Xenopus* oocytes expressing LGC-57, LGC-58a, LGC-40, and LGC-49,
627 oocytes were perfused for 10s with a panel of ligands each at 1mM: ACh (acetylcholine), Ch
628 (choline), Bet (betaine), TA (tyramine), DA (dopamine), 5-HT (serotonin), OA (octopamine),
629 GA (GABA), GLU (glutamate), His (histamine), MA (melatonin). (**B**) Phylogenetic tree of a
630 subgroup of Cys-loop ligand gated ion channels in *C. elegans*, groups of interest are highlighted
631 by colour: 'ACC' group of acetylcholine gated channels (red), orphan 'cationic diverse' group
632 (yellow), orphan LGC-57 group (green). Gene names in bold are deorphanised in this study.
633 (**C**) Dose response curves for LGC-57, LGC-58a, LGC-40 and LGC-49 in response to their
634 major ligand(s). Current is normalised by I/Imax for each oocyte, for LGC-49 current is raw
635 un-normalised current. Error bars represent SEM of 5-14 oocytes. Curves are fitted with a four-
636 parameter variable slope, inserts show EC_{50} in μM for each ligand.

637

638 **Figure 2. Ion Selectivity and Antagonistic Characterisation of Cholinergic LGICs. (A)**
639 Representative current voltage plots of newly de-organised channels in ND96, Na gluconate or
640 NMDG solutions. Current was normalised by subtraction of leak current (in absence of
641 activating ligand) and to the peak current for each oocyte. (**B**) Box plot of ΔE_{rev} of NMDG and
642 Na Gluconate vs. ND96 in oocytes expressing LGC-57, LGC-58a, LGC-40, LGC-39, LGC-
643 46, and LGC-49, E_{rev} was calculated in the presence of the major agonist of each channel and

644 leak subtracted. N=6-11 oocytes. (**C**) Current ratio of oocytes expressing LGC-57, LGC-58,
645 LGC-46, LGC-49 or LGC-39 undergoing repeated agonist application with 10s, 30s and 60s
646 wash intervals. Error bars represent SEM. N=5-9 oocytes per condition. (**D**) Antagonist
647 application in the presence of ligands using mecamylamine, strychnine, tubocurarine and
648 picrotoxin. Current is normalised by I/Imax for each oocyte, curves are fitted with a three-
649 parameter variable slope, error bars represent SEM of 2-7 oocytes, inserts show IC_{50} in μM for
650 each antagonist.
651
652 **Figure 3. LGC-39 Forms a Polymodal Ligand-Gated Ion Channel.** (**A**) Continuous current
653 trace of a *Xenopus* oocyte clamped at -60mV expressing LGC-39, perfused during 10s pulses
654 with a panel of ligands each at 1mM: ACh (acetylcholine), Ch (choline), Bet (betaine), Tyr
655 (tyramine), DA (dopamine), 5-HT (serotonin), Oct (octopamine), GA (GABA), Glu
656 (glutamate), His (histamine). (**B**) Dose response curve for LGC-39 in response to ACh, Oct
657 and Tyr. Current is normalised by I/Imax for each oocyte. Error bars represent SEM of 8-12.
658 Curves are fit with four-parameter variable slope, inserts show EC_{50} in μM for each ligand. (**C**)
659 Current-voltage relationship during recordings in NMDG, Na Gluconate or ND96 in oocytes
660 expressing LGC-39. Insert shows ΔErev vs. ND96 in mV +/- SEM of 5 oocytes. (**D**) Antagonist
661 dose response curves for LGC-39 expressing oocytes activated by either ACh, Oct or no ligand
662 at a constant dose and varying doses of mecamylamine, strychnine and tubocurarine. Error bars
663 represent SEM of 3-7 oocytes. Curves are fit with X, inserts show IC_{50} in μM for each ligand.
664 (**E**) Three different agonists do not differ in how they influence the ability for LGC-39 to be
665 stimulated with short time intervals after repeated stimulation.
666
667 **Figure 4. Newly Deorphanised LGICs are Expressed Broadly in the Nervous System. (A-**
668 **E)** Fluorescent reporters of intercistonically spliced mKate2 or GFP driven under the promoter

669 and/or genomic sequence of reveals broad neuronal expression of cholinergic channels with
670 little overlap. (**F**) Schematic depicting a subset of the synaptic connections received by the *lgc-*
671 *39* expressing neuron class, AVA, numbers in brackets show the total number of synapses for
672 each connection.
673
674 **Figure 5. Predicting Synapse Polarity Based on LGIC Expression.** (**A**) Bar chart depicting
675 the percentage of total neuron classes expression inhibitory, excitatory, both or no receptors
676 for GABA, glutamate (Glu) and acetylcholine (ACh). (**B**) Bar chart depicting the percentage
677 of total synapses for a given neurotransmitter that are predicted to be inhibitory, excitatory or
678 have no prediction. (**C**) Network diagram depicting the polarity of synaptic connections
679 between neuron classes, connection colour shown polarity: teal (inhibitory), pink (excitatory),
680 grey (no prediction). Gap junctions are represented by dashed lines. Line weight represents
681 number of synapses and nodes are coloured by the major neurotransmitter a class release.
682 Diagram made with cytoscape using the EntOpt clustering package. (**D**) Network diagram
683 depicting the predicted polarity of the locomotion circuit, connection colour shows polarity:
684 teal (inhibitory), pink (excitatory), grey (no prediction). Inserts show the fold magnitude of
685 expression of the major receptor type for each neurotransmitter in each neuron class. Gap
686 junctions are represented by dashed lines. Line weight represents number of synapses and
687 nodes are coloured by the major neurotransmitter a class release. Diagram made with
688 cytoscape.
689
690 **Figure 6. Correlation of cholinergic synapses with expression pattern of cholinergic ion**
691 **channels.** (**A-B**) Heatmaps showing expression level of newly deorphanised LGICs in each
692 neuron class. Neurons are sorted by the total number of cholinergic synapses they make (top,
693 'ACh Out') or receive (bottom, 'ACh In'). (**C-F**) Scatter plots showing correlation between

694 the total number of cholinergic synapses made (orange) or received (red) by a neuron and
695 expression of *lgc-49, acc-1*, *lgc-40* or *lgc-46*.
696
697 **Figure 7. Protein expression pattern of cholinergic ion channels.** (**A-D**) Localisation of
698 endogenously GFP tagged LGC-39, LGC-40, LGC-57 and LGC-58. White arrows highlight
699 areas of interest, represented in higher magnification below.
700

701 ## Expanded View Figure Legends

702
703 Supplementary Table 1: **The list shows ligand identity and ion selectivity for LGICs in *C.***
704 ***elegans*. For orphan receptors the ligand has been predicted based on homology, this**
705 **has been noted in the list.**
706
707 Supplementary Table 2: **List of *C. elegans* strains used in this study**
708
709 Supplementary Figure 1: **Negative traces for still orphan LGICs, ion selectivity**
710 **representative curves and channel kinetics.**
711 A. Continuous TEVC traces from oocytes clamped at -60mV expressing LGC-32, LGC-33,
712 LGC-34, LGC-42, LGC-44, and LGC-48, exposed to 10s of a panel of ligands. B. LGC-47 and
713 ACC-1 do not form a heteromeric channel in Xenopus oocytes. Left: Acetylcholine induced
714 dose response curves for oocytes expressing ACC-1 alone or in combination with LGC-47.
715 Error bars represent SEM of 7-12 oocytes per construct, insert shows EC_{50} values. Right:
716 Continuous TEVC traces from oocytes clamped at -60mV expressing LGC-47, ACC-1 or a
717 combination, exposed to 10s of a panel of ligands.
718

719 Supplementary Figure 2: **Expression patterns of still orphan LGICs, and *in vitro* data for**
720 **functional GFP tagged LGICs.**
721 A. Expression of fluorescent reporters for still orphan LGCIs. B. Acetylcholine induced dose
722 response curve, continuous trace, and expression pattern of LGC-46. Error bars represent SEM
723 of 6 oocytes. Insert shows EC_{50}. Dose response curves for GFP tagged LGICs in response to
724 their major activating ligands. Error bars represent SEM of 4-5 oocytes per construct, inserts
725 show EC_{50}. C. Expression of fluorescent reporters for plgc-46 shows a broad neuronal
726 expression pattern with expression in e.g., AIZ, RIH and AVE.
727
728 Supplementary Figure 3: **Binary heatmap of synaptic sign prediction for the three major**
729 **neurotransmitters; ACh, glutamate and GABA**. The heatmap shows the summed
730 expression level of all LGICs in *C. elegans* per neuron and transmitter, a net sum of
731 excitatory channels is displayed in red, inhibitory in green, equal expression in peach and no
732 expression of LGICs in white.
733
734 Supplementary Figure 4: **Expression heatmap for the three major neurotransmitters**
735 The heatmap shows the summed expression level, and ion selectivity, for LGICs separated by
736 transmitter (ACh, glutamate and GABA) and neuron class. Net excitatory channel expression
737 is represented in pink and inhibitory in green.
738
739 Supplementary Figure 5: **Correlation graphs between cholinergic synapses and**
740 **expression of selected LGICs.**
741 Scatter plots showing gene expression level vs total no. cholinergic synapses received (red)
742 and made (orange). Lines fit using relplot with shaded areas representing the standard error of
743 the line fit.

744

745 Supplementary Figure 6: **GFP tagging of LGICs does not influence channel function**.

746 Acetylcholine or choline induced dose response curves for oocytes expressing GFP tagged

747 version of LGC-40, LGC-57 and LGC-58 shows that EC_{50} values are not influenced by the

748 insertion of the GFP tag. Error bars represent SEM of 7-12 oocytes per construct, insert shows

749 EC_{50} values.

750

751

752 **Figures:**

753 Figure 1

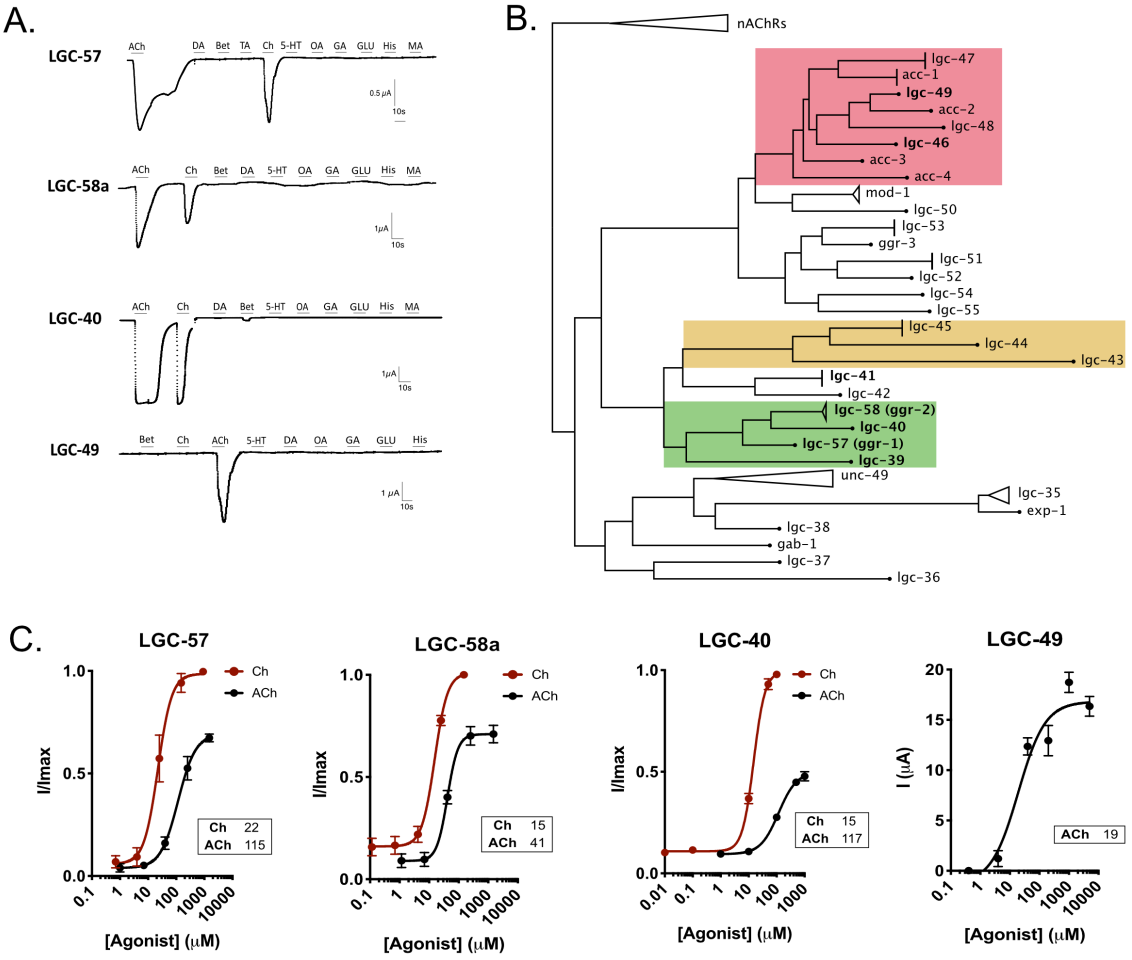

754

755 Figure 2

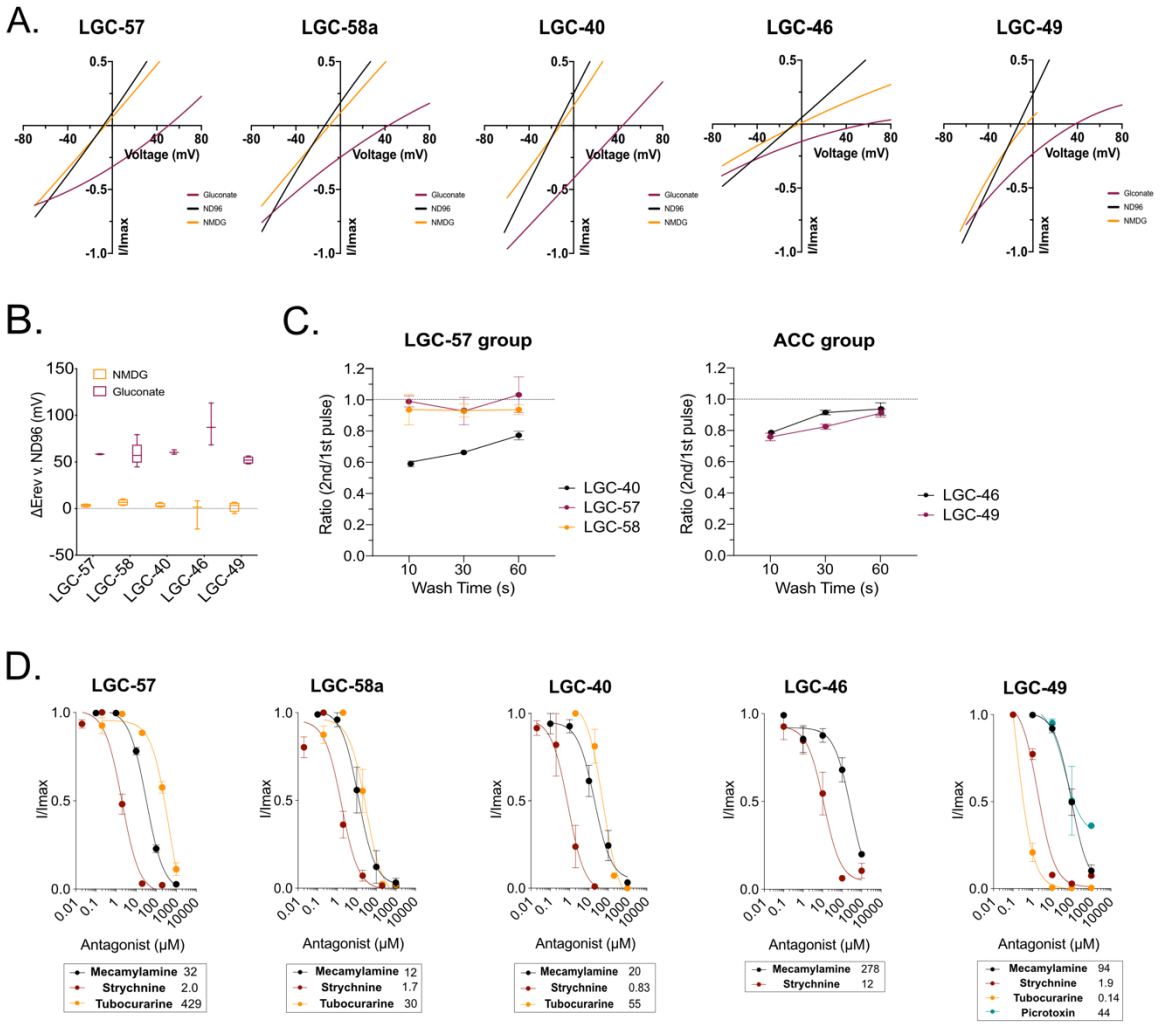

756

Figure 3

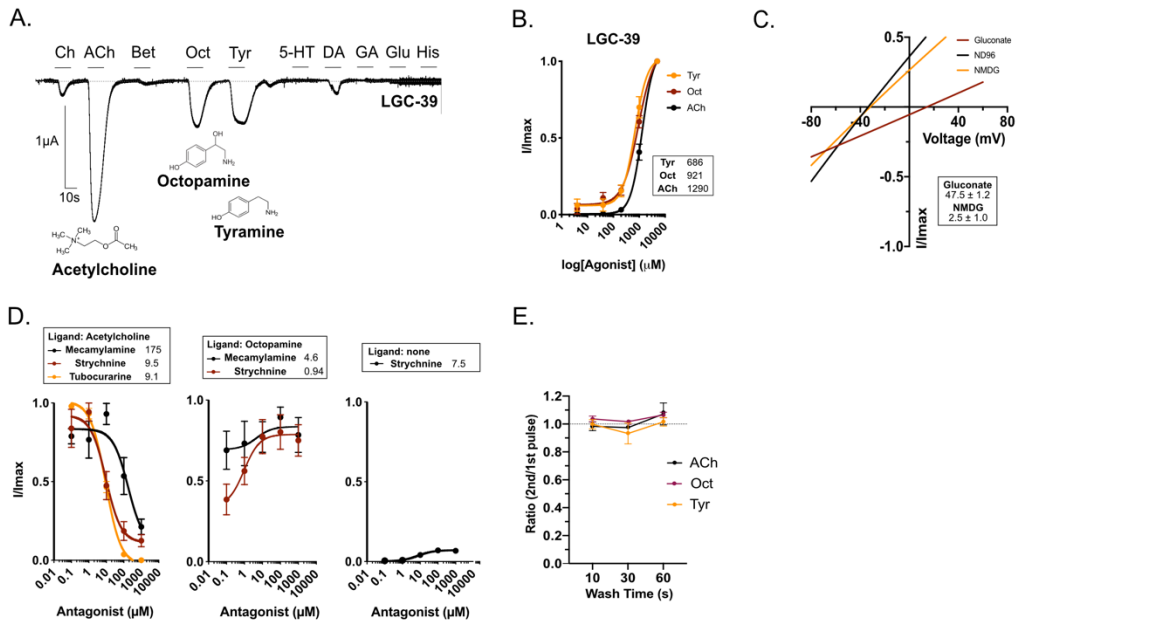

Figure 4

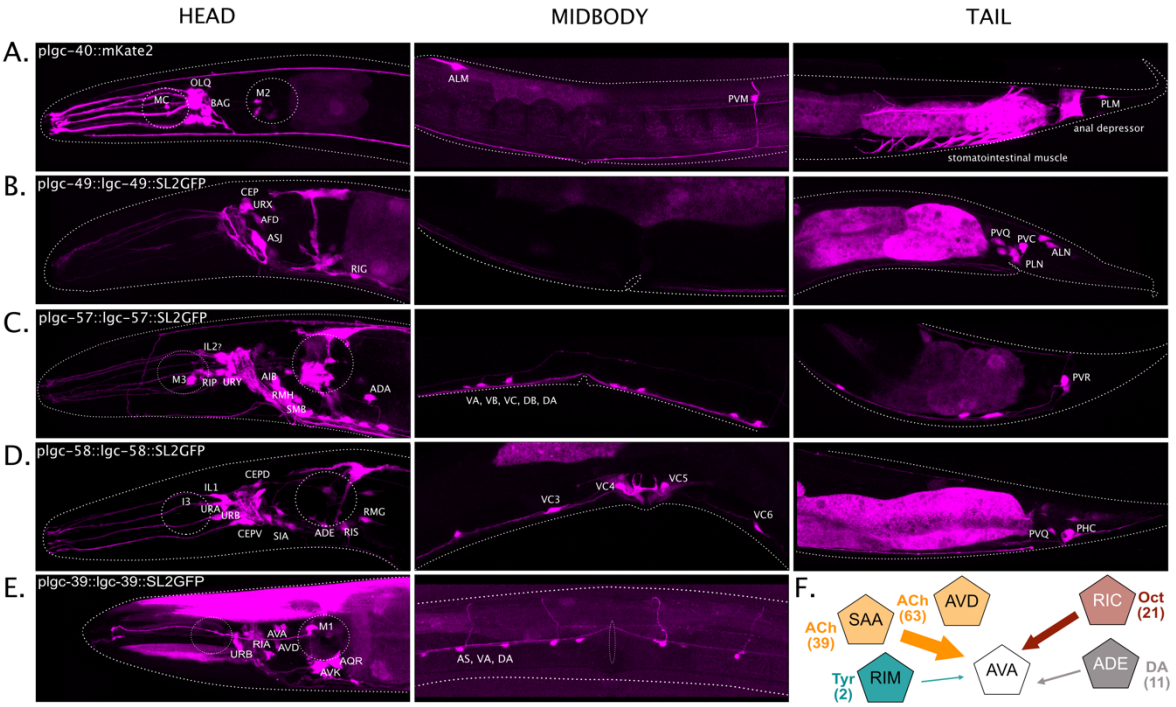

Figure 5

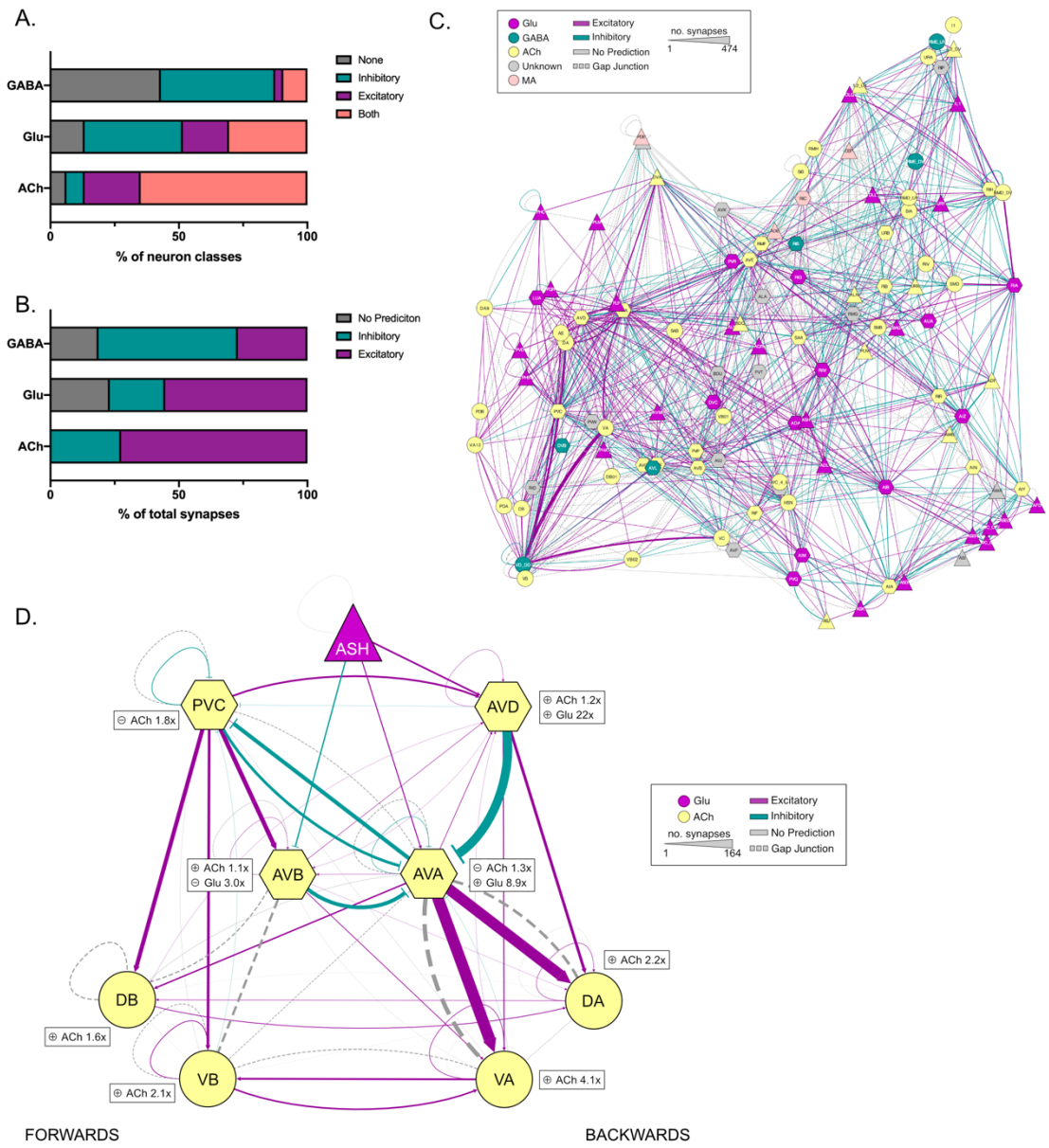
A.
GABA
Glu
ACh
0
50
100
% of neuron classes
None
Inhibitory
Excitatory
Both
B.
GABA
Glu
ACh
0
50
100
% of total synapses
No Prediciton
Inhibitory
Excitatory
C.
Glu
GABA
ACh
Unknown
MA
Excitatory
Inhibitory
No Prediction
Gap Junction
no. synapses
1
474
D.
ASH
PVC
AVD
AVB
AVA
DB
DA
VB
VA
⊖ ACh 1.8x
⊕ ACh 1.2x
⊕ Glu 22x
⊕ ACh 1.1x
⊖ Glu 3.0x
⊖ ACh 1.3x
⊕ Glu 8.9x
⊕ ACh 2.2x
⊕ ACh 1.6x
⊕ ACh 2.1x
⊕ ACh 4.1x
Glu
ACh
Excitatory
Inhibitory
No Prediction
Gap Junction
no. synapses
1
164
FORWARDS
BACKWARDS

Figure 6

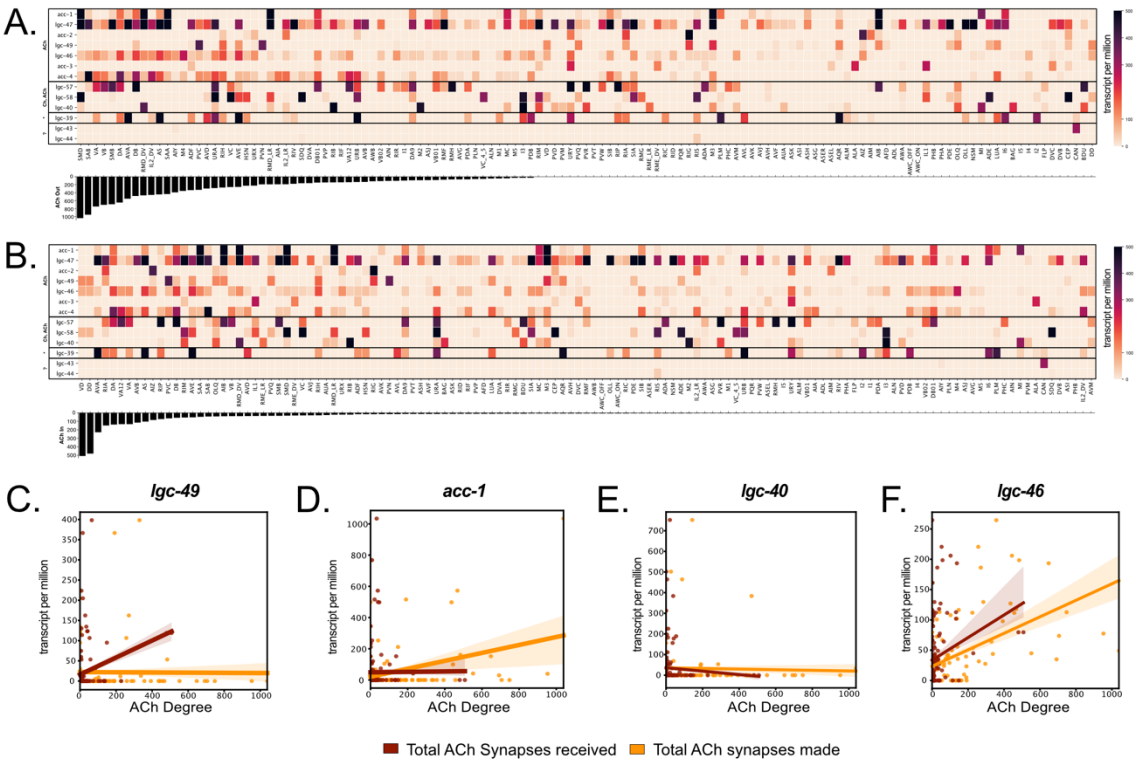
A.
B.
transcript per million
C.
lgc-49
D.
acc-1
E.
lgc-40
F.
lgc-46
transcript per million
ACh Degree
Total ACh Synapses received
Total ACh synapses made

Figure 7

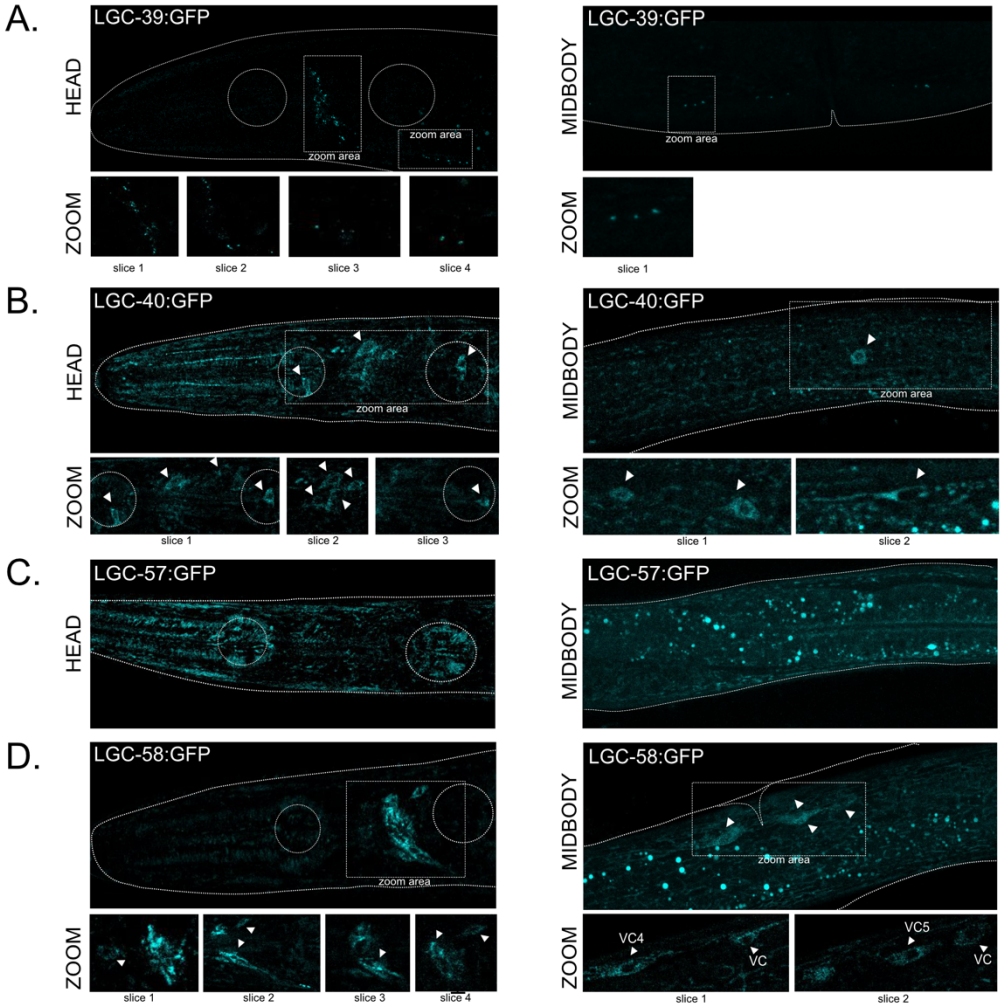
A.
LGC-39:GFP
HEAD
zoom area
zoom area
ZOOM
slice 1
slice 2
slice 3
slice 4
LGC-39:GFP
MIDBODY
zoom area
ZOOM
slice 1
B.
LGC-40:GFP
HEAD
zoom area
ZOOM
slice 1
slice 2
slice 3
LGC-40:GFP
MIDBODY
zoom area
ZOOM
slice 1
slice 2
C.
LGC-57:GFP
HEAD
LGC-57:GFP
MIDBODY
D.
LGC-58:GFP
HEAD
zoom area
ZOOM
slice 1
slice 2
slice 3
slice 4
LGC-58:GFP
MIDBODY
zoom area
ZOOM
VC4
VC
VC5
VC
slice 1
slice 2